Comfortable Helicopter Flight Via Passive/Active Morphing

TUGRUL OKTAY
Erciyes University
Kayseri, Turkey

CORNEL SULTAN
Virginia Tech
Blacksburg, VA, USA

This article offers a new perspective in defining comfortable helicopter flight along with two solutions based on passive and active main rotor morphing. Constrained optimization design problems aimed at minimizing flight control energy while satisfying variance constraints on flight parameters that are considered important in passenger comfort and noise reduction are formulated and solved. Output variance constrained (OVC) control is used for control system design and simultaneous perturbation stochastic approximation (SPSA) is employed to solve the resulting constrained optimization problems. Details on the computation of the control energy are given. Closed-loop responses of designs that satisfy prescribed variance constraints with a very small margin on the achievable variance bounds are compared with responses of designs that satisfy such constraints with a larger margin both for passively and actively morphing helicopters.

Manuscript received July 1, 2014; revised February 14, 2015; released for publication May 15, 2015.

DOI. No. 10.1109/TAES.2015.140488.

Refereeing of this contribution was handled by L. Rodrigues.

Authors' addresses: T. Oktay, Faculty of Aeronautics and Astronautics, Erciyes University, Kayseri 38030, Turkey. E-mail: (tugruloktay52@gmail.com). C. Sultan, Department of Aerospace and Ocean Engineering, Virginia Tech, Blacksburg, VA 24060.

NOMENCLATURE

p, q, r	=	Helicopter angular velocities, [deg/s]
u, v, w	=	Helicopter linear velocities, [m/s]
ϕ_A, θ_A, ψ_A	=	Helicopter Euler angles, [deg]
c_b	=	Blade chord length, [m]
κ_β	=	Blade flapping spring stiffness coefficient, [Nm/rad]
J	=	Control energy (cost)
m	=	Blade linear mass density, [kg/m]
R	=	Blade length, [m]
$\beta_0, \beta_c, \beta_s$	=	Collective and two cyclic blade flapping angles, [deg]
$\zeta_0, \zeta_c, \zeta_s$	=	Collective and two cyclic blade lagging angles, [deg]
$\theta_0, \theta_c, \theta_s$	=	Collective and two cyclic blade pitch angles, [deg]
θ_{tw}	=	Blade twist, [deg]
θ_T	=	Collective tail rotor angle, [deg]
Ω	=	Main rotor angular speed, [deg/s]

I. INTRODUCTION

In the early years of helicopter flight, pilot/passenger comfort was of minimal importance compared with flight safety. It is clear that the comfort is directly related to the helicopter vibration/noise level, so reduction of these parameters in helicopter flight will naturally improve the comfort level experienced by passengers and decrease the pilot stress level. In this article we attempt to address the comfort improvement problem from this point of view, as a problem in reduced vibration/noise via multivariable, constrained control design.

Helicopter noise reduction is a topic of research in designing helicopters that can be operated more quietly, reducing the public-relations problems with night flying, operating or expanding an airport. Noise reduction is of course essential for military applications in which stealth is required: long-range propagation of helicopter noise can alert an enemy in time to reorient defenses. Helicopter noise/vibration reduction also improves passenger/pilot comfort and reduces the stress/workload of the pilot.

There have been many research papers published on noise/vibration reduction [1–8]. For example in [3], control of vibration and required rotor power is implemented with partial span trailing edge flaps operating according to a closed-loop control algorithm. In another study [6], vibratory loads at the rotor hub, which are the main sources of helicopter vibration, are reduced by redesigning the helicopter using certain variables (e.g., blade lag and torsion stiffness). This also improves passenger comfort. There is also one other way of improving comfort. Specifically, it is intuitive that by reducing the Euler angle perturbations the comfort level will increase [9–12]. In all comfort improvement strategies active control is a critical enabling technology, therefore a review of helicopter control is mandatory.

Throughout the years many strategies for aircraft flight control system (FCS) design have been investigated. Some of these techniques, listed here in approximate historical order are: classical pole placement method and simple feedback approaches [13–18], adjusted linear quadratic regulator (LQR) and linear quadratic Gaussian (LQG) controllers [19–21], modified H_∞ control synthesis [22–24], constrained model predictive control (MPC) [25–27], and variance constrained controllers [9–12, 28–32]. In [33] the feasibility of nonlinear robust control based on Lyapunov functions was recently demonstrated in rotorcraft control. Variance constrained controllers, which have been only recently studied, specifically for helicopter sensor failure management [28] and passive [10] and active [12] blade morphing control, will be the focus of this article. These controllers are LQG controllers which guarantee satisfaction of certain variance constraints. And they utilize second-order information (i.e., state covariance matrix, see [34, 35] for more information).

Variance constrained controllers have been used for some aerospace vehicles control before (e.g. helicopters [9–12, 28–31]; tiltrotor aircraft, [32], Hubble space telescope [36], and tensegrity structures [37, 38]). For example, in [28] variance constrained controllers were applied for helicopter FCS during specific maneuvers (i.e., level banked turn and helical turn). Moreover, in [10] variance constrained controllers were applied for passively blade morphing helicopters. In another study [12] output variance constrained (OVCs) controllers were applied for actively blade morphing helicopters. The major difference between the active and the passive morphing study in [10] is that in the active case the helicopter design parameters are used as FCS parameters so they vary during flight, but in a prescribed interval ($+/-5\%$ of their nominal values). However, in the passive case the helicopter design parameters do not vary during flight (i.e., straight level flight or maneuvering flight). Passive as well as active morphing requires changes in some helicopter parameters (e.g., blade length, blade chord, etc.). The key difference is that active morphing requires continuous measurements and actuation as well as a feedback control mechanism whereas passive morphing does not. Passive morphing changes can be applied by engineers and technicians, for example as a one time change before the helicopter begins the flight mission or even at some point during flight. Once applied, these changes remain fixed for a prolonged period of time during flight. Therefore, passive morphing does not involve additional actively controlled elements beyond the four conventional helicopter controls (i.e. blade pitch collective, two cyclics, and tail rotor). In contrast, active morphing requires special mechanisms that enable continuous, in-flight modification of some of the helicopter parameters. These modifications are computed in response to sensor measurements and implemented via feedback control. Therefore, active morphing involves additional feedback controlled parameters beyond the four conventional helicopter controls. Clearly, passive morphing is easier to implement since it does not require additional feedback-driven actuation mechanisms, whereas active morphing requires sophisticated onboard signal processing, multivariable, large dimensional controllers, rapid continuous actuation mechanisms, as well as computational power. However, active morphing is generally expected to yield significant improvement in all aspects of helicopter flight performance.

In this article, to improve flight comfort, we apply both passive and active blade morphing control as well as simultaneous design (i.e., of the helicopter and control system) to highly complex helicopter models that include relevant physics for helicopter flight control. Specifically we use an analytical formulation for fuselage aerodynamics, including degrees of freedom for blade flapping and lead-lagging motions, aerodynamics of tail rotor and empennage, downwash of main rotor, landing gear effects, etc. The main viewpoint of our modeling process is to build up physics-based, control-oriented models capturing the "essential dynamics." By essential dynamics we mean, not only the dynamics to be controlled, but also dynamic effects that are directly affected by control system design and which are crucial for safe and performant helicopter operation. For instance, even if the principal objective of the control system design is to control flight dynamics modes, we are interested to capture blade flapping and blade lead-lagging modes and monitor their behavior in the closed-loop configuration. Of course, development of such models necessitates a multibody dynamics approach which has been presented in detail in [9]. References [12] and [29] also show how the validity of these models has been confirmed against trim and dynamics data that is available in the published literature.

The problem of simultaneous design obtained via joining our helicopter models and dynamic feedback variance controllers is a highly complex constrained optimization problem, which does not permit analytical computation of derivatives (e.g. gradients or/and Hessians that are necessary in traditional optimization approaches). Therefore, we have chosen a stochastic optimization method, which is called simultaneous perturbation stochastic approximation (SPSA), to solve the optimization problem. SPSA was selected primarily due to its previous success in rapidly solving similar, highly complex and constrained optimization problems [40, 41].

In this article achievable bounds of OVC are considered for the first time in passive and active blade morphing helicopters control. Closed-loop responses of designs that satisfy prescribed variance constraints with a very small margin (i.e., actual variances are very close to the achievable bounds) are compared with responses of designs that satisfy these constraints with a larger margin both for passively and actively morphing helicopters. Therefore this study is different than previous studies in [10] and [12], since it focuses on achievable bounds for passive/active morphing rather than only studying

arbitrarily specified variance bounds. Vibration/noise reduction is also for the first time considered in this paper, in conjunction with variance control design.

For the conventional helicopter, there are two fundamental systems that contribute to the generation of near-field and far-field noise, the main rotor and the tail rotor. It has been long established that noise intensity is directly related to typical angles associated with rotor blades (pitch, flapping, lead-lagging). In general the larger these angles are the larger the noise intensity is. Therefore, it is reasonable to enforce the condition that some if not all of these angles amplitudes are reduced for improved comfort/reduced noise intensity. This is the line of thought we follow in this article. For example, control design can be used to decrease variances of the control angles (i.e. blade pitch angles) by minimizing control energy while keeping flapping and lead-lagging angles small by satisfying prescribed variance bounds.

II. HELICOPTER MATHEMATICAL MODEL

Our modeling approach depends on two main points. First, physics principles and suitable modeling assumptions are used to result in nonlinear ordinary differential equations (ODEs). Second, the models include not only the flight dynamics modes but also blade dynamics modes that are critical for safe and performant operation. To obtain such models multibody dynamics was used to capture all important components of a helicopter: fuselage, fully articulated main rotor with 4 blades, empennage, landing gear, tail rotor. The key points in obtaining the model are given next.

A. Dynamic and Kinematic Equations of Fuselage

To find the nondimensionalized helicopter force and moment equations (1) and (2) Newton-Euler equations were used giving

$$\begin{aligned}
&\frac{d}{d\psi}\hat{u}+\hat{q}\hat{w}-\hat{r}\hat{v}+\frac{g\sin(\theta_A)}{\Omega^2 R}=\frac{X}{\Omega^2 R M_a}\\
&\frac{d}{d\psi}\hat{v}+\hat{r}\hat{u}-\hat{p}\hat{w}-\frac{g\cos(\theta_A)\sin(\phi_A)}{\Omega^2 R}=\frac{Y}{\Omega^2 R M_a}\\
&\frac{d}{d\psi}\hat{w}+\hat{p}\hat{v}-\hat{q}\hat{u}-\frac{g\cos(\theta_A)\cos(\phi_A)}{\Omega^2 R}=\frac{Z}{\Omega^2 R M_a}
\end{aligned} \tag{1}$$

$$\begin{aligned}
&\frac{d}{d\psi}\hat{p}-\hat{q}\hat{r}\left(\frac{I_{yy}}{I_{xx}}-\frac{I_{zz}}{I_{xx}}\right)-\frac{I_{xz}}{I_{xx}}\left(\hat{p}\hat{q}+\frac{d}{d\psi}\hat{r}\right)=\frac{L}{I_{xx}\Omega^2}\\
&\frac{d}{d\psi}\hat{q}-\hat{p}\hat{r}\left(\frac{I_{zz}}{I_{yy}}-\frac{I_{xx}}{I_{yy}}\right)+\frac{I_{xz}}{I_{yy}}\left(\hat{p}^2-\hat{q}^2\right)=\frac{M}{I_{yy}\Omega^2}\\
&\frac{d}{d\psi}\hat{r}-\hat{p}\hat{q}\left(\frac{I_{xx}}{I_{zz}}-\frac{I_{yy}}{I_{zz}}\right)-\frac{I_{xz}}{I_{zz}}\left(\hat{q}\hat{r}-\frac{d}{d\psi}\hat{p}\right)=\frac{N}{I_{zz}\Omega^2}
\end{aligned} \tag{2}$$

Here typical notations are used. For instance, R and ψ are blade length and azimuth angle, I is inertia matrix, M_a is the mass of the helicopter, g is the constant gravitational acceleration at sea level, and $\hat{}$ denotes the nondimensionalized quantity (see [9] for details). The nondimensionalized kinematic Euler equations are

$$\begin{aligned}
\hat{p}&=\frac{d}{d\psi}\phi_A-\frac{d}{d\psi}\psi_A\sin(\theta_A)\\
\hat{q}&=\frac{d}{d\psi}\psi_A\cos(\theta_A)\sin(\phi_A)+\frac{d}{d\psi}\theta_A\cos(\phi_A)\\
\hat{r}&=\frac{d}{d\psi}\psi_A\cos(\theta_A)\cos(\phi_A)-\frac{d}{d\psi}\theta_A\sin(\phi_A)
\end{aligned} \tag{3}$$

B. Dynamic and Aerodynamic Forces Acting on Single Blade

The infinitesimal aerodynamic force and moment acting on a blade strip in lead-lagging and flapping frame (LLF) are, respectively, (see [9])

$$d_{LLF}F_{aero}=\frac{\gamma I_b}{2R^3}\begin{bmatrix}0\\ -\left(\theta U_T^2-U_P U_T\right)\frac{U_P}{U_T}-\frac{1}{a_0}\left(\delta_0+\delta_2\left(\theta-\frac{U_P}{U_T}\right)^2\right)\\ \theta U_T^2-U_P U_T\end{bmatrix}dx \tag{4}$$

$$d_{LLF}M_{aero}=\begin{bmatrix}0 & -xR\left(d_{LLF}F_{aero}\right)_{III} & xR\left(d_{LLF}F_{aero}\right)_{II}\end{bmatrix}^T \tag{5}$$

Here U_P and U_T are perpendicular and tangential components of air velocity acting on the blade leading edge, $\theta$is the blade pitch angle, x is the nondimensional location of a generic point on the blade, $\gamma$is the Lock number, a_0 is the blade lift curve slope, and δ_0 and δ_2 are parasite and induced drag coefficients. Integration over the blade length gives total blade aerodynamic force and moment.

C. Multiblade Equations

Neglecting higher harmonic terms and using 4 blades for the main rotor, the blade flapping and lead-lagging motions are expressed by

$$\Theta_i(\psi)=\Theta_0+\Theta_{1c}\cos(\psi_i)+\Theta_{1s}\sin(\psi_i)+\Theta_{0d}(-1)^i \tag{6}$$

where the blade azimuth angle of the blade i is

$$\psi_i=\psi-\left(\pi/2\right)(i-1),\quad i=1,\ldots,4 \tag{7}$$

and Θ is the generic notation for any of the two angles mentioned in the above while Θ_0, Θ_c, Θ_s, and Θ_d are collective, two cyclic and differential components, respectively (see [42, pp. 102–106] for synchronous flapping motion discussion). Each blade motion is derived by using the relevant azimuth angle (see (7)).

D. Downwash of Main Rotor

A linear static inflow model was chosen for the downwash. Its cyclic components λ_c, λ_s are (see [43, p. 160]):

$$\lambda_c = \lambda_0 \frac{15\pi}{23} \tan\left(\frac{\chi}{2}\right), \quad \lambda_s = 0, \quad \chi = \tan^{-1}\left(\frac{\hat{u}}{\hat{w} + \lambda_0}\right) \tag{8}$$

where χ is the wake skew angle. The uniform component of the linear inflow λ_0 is calculated numerically using the momentum theory (see [9]).

E. Tail Rotor

The tail rotor does not flap and is not canted, and its induced inflow is ignored. Its effect is a force in antitorque direction. The drag force due to the tail rotor hub and shaft is also modeled (see [9] for more details).

F. Assembly

For the aggregate helicopter model all the components outlined in the above were assembled into the nonlinear equations of the helicopter dynamics. These, derived using Maple, were obtained in the generic implicit form

$$f(\dot{x}, x, \upsilon) = 0 \tag{9}$$

where $f \in \mathbb{R}^{28}$, $x \in \mathbb{R}^{25}$ is the nonlinear state vector comprising the fuselage states (i.e., linear and angular velocities, Euler angles) and blade states (i.e., flapping and lead-lagging states), and $\upsilon \in \mathbb{R}^4$ is the nonlinear control vector comprising two cyclic and a collective control for the main rotor and tail rotor force (see [9] for details). For control design the nonlinear model was linearized around several trim conditions. The trim conditions were found using "fsolve" in Matlab to solve the resulting algebraic equations and linearization was performed in Maple. Reference [44] provides examples of the linear model matrices for some specific flight conditions.

III. HELICOPTER FLIGHT CONTROL SYSTEM

In this article for helicopter control we use output variance constrained controllers (OVC). In the following we review key elements related to OVC such as energy and variance computation.

A. Energy Computation for LQG/OVC

Consider a continuous first-order linear time invariant (LTI), stabilizable and detectable system, which we call the "plant"

$$\begin{aligned} \dot{x}_p(\mathrm{t}) &= A_p x_p(\mathrm{t}) + B_p \mathrm{u}(\mathrm{t}) + w_p(\mathrm{t}), \\ y_p(\mathrm{t}) &= C_p x_p(\mathrm{t}), \quad z(\mathrm{t}) = M_p x_p(\mathrm{t}) + v(\mathrm{t}) \end{aligned} \tag{10}$$

and a full-order dynamic controller

$$\dot{x}_c(\mathrm{t}) = A_c x_c(\mathrm{t}) + F z(\mathrm{t}), \quad \mathrm{u}(\mathrm{t}) = G x_c(\mathrm{t}) \tag{11}$$

Here y_p is the vector of size n_y of system outputs, z is the vector of sensor measurements of size n_z, w_p and v are zero-mean uncorrelated process and measurement Gaussian white noises with intensities W_p and V, respectively, and x_c is the controller state vector of the same size n as the plant state vector x_p. Matrices F and G are state estimator and controller gain, respectively. Then, with the closed-loop state defined as $x(t) = [\, x_p^T(\mathrm{t})\ x_c^T(\mathrm{t})\,]^T$, the closed-loop system is

$$\dot{x}(t) = Ax(t) + Dw(t), \ \ y(t) = Cx(t) \tag{12}$$

where

$$A = \begin{bmatrix} A_p & B_p G \\ F M_p & A_c \end{bmatrix}, \ D = \begin{bmatrix} D_p & 0 \\ 0 & F \end{bmatrix}, \ W = \begin{bmatrix} W_p & 0 \\ 0 & V \end{bmatrix}$$

and the output is

$$y(t) = \begin{bmatrix} y_p(t) \\ \mathrm{u}(t) \end{bmatrix} = \begin{bmatrix} C_y \\ C_{\mathrm{u}} \end{bmatrix} x(\mathrm{t}) \tag{13}$$

where $C_y = [\, C_p\ 0\,]$ and $C_{\mathrm{u}} = [\, 0\ G\,]$. It is assumed that the closed-loop system is exponentially stable. Then, for this definition of the closed-loop state, the control energy, defined as

$$J = E_\infty \mathrm{u}^T R \mathrm{u} \tag{14}$$

where $E_\infty \triangleq \lim_{t\to\infty} E$ with E the expectation operator, is computed as

$$J = tr\left(R C_{\mathrm{u}} X C_{\mathrm{u}}^T\right) \tag{15}$$

where tr is the trace and

$$X = \begin{bmatrix} X_{11} & X_{12} \\ X_{21} & X_{22} \end{bmatrix} \tag{16}$$

is the "steady state" closed-loop state covariance matrix that can be computed by solving the following Lyapunov equation:

$$0 = AX + XA^T + DWD^T \tag{17}$$

Note that the size of this Lyapunov equation is twice the size of the plant (for example, the size of matrix A is 50×50 for our helicopter model, i.e. $n = 25$). Simple algebra performed on (17) shows that

$$J = tr(RGX_{22}G^T) \tag{18}$$

Therefore only the lower right part of X is required to compute the control energy.

If the dynamic controller is an LQG controller, it can be shown (for example by defining the closed-loop state as $\bar{x}(t) = [\, x_p^T(\mathrm{t}) - x_c^T(\mathrm{t})\ x_c^T(\mathrm{t})\,]^T$) and using the LQG optimality conditions) that X_{22} (which is the covariance matrix of the controller state) can be evaluated by solving a smaller size Lyapunov equation:

$$0 = X_{22}\left(A_p + B_p G\right)^T + \left(A_p + B_p G\right) X_{22} + F V F^T \tag{19}$$

For large dimensional systems, solving (19) may be an important computational advantage compared with solving (17).

B. Computation of Variances

Let $y_i(t)$ be one of the components of $y(t)$ in (13). The variance of $y_i(t)$ is defined by

$$Y_i = E_\infty \left\{ y_i^2 \right\} \tag{20}$$

and if $1 \le i \le n_y$ it represents an "output variance" while if $n_y + 1 \le i \le n_y + n_u$ it represents an "input variance." These variances can also be calculated using some parts of the steady state closed-loop covariance matrix.

$$E_\infty y_{pi}^2 = [Y]_{ii},\ for\ i \le n_y \tag{21a}$$

$$E_\infty \mathrm{u}_i^2 = [Y]_{ii},\ for\ i \ge n_y + 1 \tag{21b}$$

where $Y = C_\mathrm{u} X C_\mathrm{u}^T$. Therefore,

$$E_\infty y_{pi}^2 = \begin{bmatrix} C_{pi}^T & 0 \end{bmatrix} \begin{bmatrix} X_{11} & X_{12} \\ X_{21} & X_{22} \end{bmatrix} \begin{bmatrix} C_{pi} \\ 0 \end{bmatrix} = C_{pi}^T X_{11} C_{pi} \tag{22}$$

$$E_\infty \mathrm{u}_i^2 = \begin{bmatrix} 0 & G_i^T \end{bmatrix} \begin{bmatrix} X_{11} & X_{12} \\ X_{21} & X_{22} \end{bmatrix} \begin{bmatrix} 0 \\ G_i \end{bmatrix} = G_i^T X_{22} G_i \tag{23}$$

where C_{pi} and G_i are the *i-th* row of C_p and G, respectively. Therefore, output variance calculation requires

$$X_{11} = E_\infty \left\{ x_p x_p^T \right\} = X_p \tag{24}$$

and input variance calculation requires

$$X_{22} = E_\infty \left\{ x_c x_c^T \right\} = X_c \tag{25}$$

C. OVC Problem

For OVC design the problem described next must be solved [45, 46]. Given (10), and an input penalty $R > 0$, find a full order dynamic controller [see (11)] to solve the problem

$$\underset{A_c, F, G}{min}\ J = E_\infty \mathrm{u}^T R \mathrm{u} = tr\left(R G X_{22} G^T \right) \tag{26}$$

subject to

$$E_\infty y_i^2 \le \sigma_i^2, \quad i = 1, ..., n_y \tag{27}$$

where σ_i^2 is the upper bound imposed on the *i-th* output variance.

The OVC solution reduces to an LQG problem by choosing output penalty $Q \ge 0$ depending on the inequality constraints. An algorithm for Q selection is presented in [45] and [46]. After converging on Q, OVC parameters are

$$\begin{aligned} A_c &= A_p + B_p G - F M_p, \quad F = \aleph M_p^T V^{-1}, \\ G &= -R^{-1} B_p^T K \end{aligned} \tag{28}$$

where $\aleph$ and K are solutions of two Riccati equations:

$$0 = \aleph A_p^T + A_p \aleph - \aleph M_p^T V^{-1} M_p \aleph + W_p \tag{29a}$$

$$0 = K A_p + A_p^T K - K B_p R^{-1} B_p^T K + C_p^T Q C_p \tag{29b}$$

Note that for all of the numerical experiments reported herein (i.e., OVCs designs and closed-loop simulations), the sensor measurements were helicopter linear velocities, angular velocities, and Euler angles. The outputs of interest were helicopter Euler angles for the first definition of comfort and blade flapping and lagging angles for the second definition of comfort. Also nondimensionalized noise intensities were taken as $W_p = 10^{-7} I_{25}$, $V = 10^{-7} I_9$ for consistency with other results used for comparison (see [29] for a discussion on the selection of these values).

It is important to note that the minimum achievable output variance bounds can be computed a priori, before OVC design is performed. These are given by

$$\left[\sigma_i^2 \right]_{min} = \left[C_p \aleph C_p^T \right]_{ii} \tag{30}$$

where, for the particular system described in (10), $\aleph$ is computed by solving the Riccati equation (29a). Therefore, before implementation of the OVC algorithm these bounds should be computed and σ_i must be selected such that $\sigma_i > \sigma_{i\,\min}$, otherwise there is no solution.

D. Problem Formulation

The passive blade morphing design problem is:

$$\underset{A_c, F, G, \Psi_p}{min}\ J = E_\infty \mathrm{u}^T\ R \mathrm{u} \tag{31}$$

subject to (10), (11), and (27) where $\Psi_p = \{c_b, \kappa_\beta, m, R, \theta_{tw}, \Omega\}$ is the set of helicopter blade optimization parameters. The elements of Ψ_p are constrained, i.e. $\Psi_{pi_{min}} \le \Psi_{pi} \le \Psi_{pi_{max}}$. Because, after solving this simultaneous helicopter and control design problem a new helicopter design is obtained along with an OVC controller, the resulting helicopter is also referred to as the redesigned helicopter (obtained via passive morphing).

Note that matrices A_p and B_p are functions of Ψ_p. These dependencies lead to a complicated optimization problem in which both the objective J and the variance constraints depend on the optimization variables in a sophisticated manner. The solution to this problem is discussed in the next section.

The active blade morphing design is summarized next. Let $\Psi_a = \{c_b, R, \theta_{tw}, \Omega\}$ be the set of trim morphing controls. The problem of obtaining optimum trim values for these morphing controls can be obtained by altering the traditional OVC design problem described in the above if we take into account the dependencies $A_p(\Psi_a)$, $B_p(\Psi_a)$. We emphasize that here Ψ_a represents the vector of morphing controls trim values. In the control problem formulation u represents perturbations of all the controls, including the morphing controls, from their trim values. The control energy in (26) as well as all the variance constraints in (27) are now functions of the trim morphing controls and the control matrices (A_c, F, G). Therefore, the following optimization problem is formulated:

$$\underset{A_c, F, G, \Psi_a}{min}\ E_\infty\ \mathrm{u}^T\ R \mathrm{u} \tag{32}$$

subject to (10), (11), and (27). In addition, the elements of Ψ_a are constrained, i.e., $\Psi_{ai_{min}} \leq \Psi_{ai} \leq \Psi_{ai_{max}}$. This new optimization problem is more complex than OVC control design and its solution is discussed next.

In order to solve the problems defined, we selected a stochastic optimization method called SPSA, which was successfully used in similar complex constrained optimization problems [9, 10, 12, 41]. SPSA is inexpensive because it uses only two evaluations of the objective to estimate the gradient [40]. It is also successful in solving constrained optimization problems [9, 10, 12, 41, 47].

IV. ACHIEVABLE BOUNDS AND COMPARISONS (COMFORT VERSION-I)

A. Passive Morphing

Using the achievable bounds equation (see (30) and [45]) it is found that $\sigma^2_{\min} = 1.3 * 10^{-7}[\,1\ 1\ 1\,]$ for the nominal helicopter. These values are close to the ones for the redesigned helicopter obtained in [10]. However, if output variance bounds very close to $\sigma^2_{\min} = 1.3 * 10^{-7}[\,1\ 1\ 1\,]$ are chosen, after solving the passive morphing design problem defined in Section IV, the expectation values of the inputs of interest are huge (e.g. $E_\infty u_i^2 > 10^{12}$, $i = 1, \ldots, 4$). This can be easily explained by the fact that tight output bounds satisfaction requires a large control effort. This is also a reflection of the trade-off one has to make between control energy and comfort requirements: the output variance specifications are directly related to improved comfort. If stringent requirements are imposed (i.e. output variance bounds close to the achievable OVC bounds) then a high price has to be paid in terms of the control effort required to achieve this level of comfort.

In [10] passive morphing was applied as described in this article using the helicopter model linearized around $V_A = 40$ kts straight level flight and some other flight conditions. For the OVC design there $\sigma^2 = 10^{-4}[\,1\ 1\ 0.1\,]$ were selected as variance constraints on Euler angles. In this study the variance constraints on Euler angles are changed to $\sigma^2 = 10^{-6}[\,1\ 1\ 1\,]$. For both articles the inputs of interest are all four conventional helicopter controls.

The relative energy saving is calculated using

$$\%J = 100\,(J_n - J_r)\big/ J_n \tag{35}$$

where J_r and J_n are the costs of OVCs obtained using the redesigned helicopter (i.e., the helicopter obtained after passive morphing) and the nominal helicopter with OVC designed to satisfy the respective OVC bounds, respectively. From [10] we have that $\%J = \%33.3$. From the current calculations we obtain a lower value, specifically $\%J = \%18.0$ (see Table I for optimum design variables). Moreover, if we use the redesigned helicopter in [10], and design a OVC controller for the new constraint (i.e. $\sigma^2 = 10^{-6}[\,1\ 1\ 1\,]$) the corresponding relative energy saving is $\%J = \%13.5$. This set of results confirms the fact that a substantial trade-off in terms of control energy must be made to satisfy stringent comfort requirements: the control energy saving went down from $\%J = \%33.3$ for $\sigma^2 = 10^{-4}[\,1\ 1\ 0.1\,]$ to $\%J = \%18.0$ and $\%J = \%13.5$ for $\sigma^2 = 10^{-6}[\,1\ 1\ 1\,]$ for two different helicopters.

TABLE I
Optimum Design Variables

	Using Old Variance Bounds [10]		Using New Variance Bounds	
	Optimum Value	Change $\Delta\Psi_{p_i}/\Psi_{p_i}$	Optimum Value	Change $\Delta\Psi_{p_i}/\Psi_{p_i}$
c_b	0.5158 m	−0.04506	0.5671 m	0.04997
K_β	50554.0426 Nm/rad	0.04995	50555.9685 Nm/rad	0.04999
m	9.5544 kg/m	0.04993	8.6458 kg/m	−0.04991
R	7.1265 m	−0.04980	7.1425 m	−0.04730
θ_{tw}	−0.1470 rad	0.04981	−0.1336 rad	−0.04525
Ω	25.6111 rad/s	−0.04996	25.6740 rad/s	−0.04911

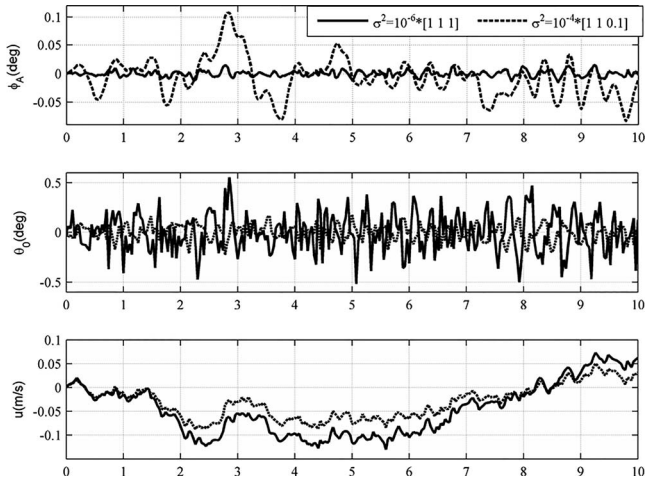

Fig. 1. Closed-loop responses of some perturbed states and controls using passive helicopter morphing for different variance bounds (comfort version-I).

For numerical simulations, several closed-loop systems are created as described next. The first closed-loop system is created using OVC designed with $\sigma^2 = 10^{-6}[\,1\ 1\ 1\,]$ for the redesigned helicopter and coupling it to the redesigned helicopter obtained using passive morphing with $\sigma^2 = 10^{-6}[\,1\ 1\ 1\,]$. The second closed-loop system is created using the OVC designed with $\sigma^2 = 10^{-4}[\,1\ 1\ 0.1\,]$ for the redesigned helicopter and coupling it to the redesigned helicopter obtained for $\sigma^2 = 10^{-4}[\,1\ 1\ 0.1\,]$. The third closed-loop system is created using OVC designed with $\sigma^2 = 10^{-6}[\,1\ 1\ 1\,]$ for the nominal helicopter and coupling it to the nominal helicopter (i.e., for which passive morphing is not used).

In Fig. 1 response of one of the helicopter Euler angle states (ϕ_A: roll angle), collective cyclic main rotor blade pitch angle and longitudinal linear velocity state (u) are given when the first closed-loop system (solid black line) and second closed-loop system (dotted black line) are both excited by white noise perturbations. From this figure it

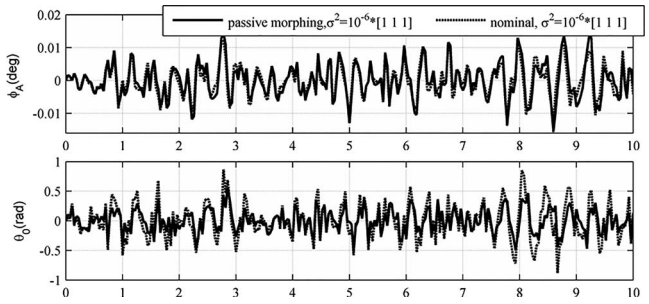

Fig. 2. Closed-loop responses of some perturbed states and controls using passive morphing versus nominal helicopter (comfort version-I).

can be easily seen that the variations of the Euler angles for the first closed-loop system are smaller than the ones for the second closed-loop system. This can be explained by the fact that the prescribed output variance bounds of the first closed-loop system are smaller than the ones of the second closed-loop system. It is worth mentioning that the very small values of these angles are expected because we enforced very small values on their variances in OVC design. Of course if larger values for the noise intensities are used in simulations, larger variations of the Euler angles are observed (here we used $W_p = 10^{-7} I_{25}$, $V = 10^{-7} I_9$ for consistency with other results). Similarly, large angle variations can be obtained if larger values for the output variance constraints are used in OVC design. However, in any case the observed pattern is qualitatively similar with the one in Fig. 1.

It can also be seen that the control variations (e.g. θ_0) from their trim values increase after using new bounds (i.e. $\sigma^2 = 10^{-6}[\,1\ 1\ 1\,]$) which are smaller than previous bounds (i.e. $\sigma^2 = 10^{-4}[\,1\ 1\ 0.1\,]$). This result confirms the expectation that smaller output variance bounds satisfaction requires larger control inputs. From this figure it can be also ascertained that other outputs (e.g. u) do not experience catastrophic behavior.

In Fig. 2 response of one of the helicopter Euler angle states (i.e. ϕ_A), and one of the main rotor controls (e.g. θ_0) are given when the first closed-loop system (solid black line) and third closed-loop system (dotted black line) are both excited by white noise perturbations. From this figure it can be easily seen that before and after redesign, the qualitative (i.e., shape of the response) and quantitative (i.e. magnitude of the response) behaviors of helicopter Euler angles are practically the same. This is explained by the fact that the variances of outputs of interest (i.e., helicopter Euler angles) are very close and satisfy the same constraints (i.e. $\sigma^2 = 10^{-6}[\,1\ 1\ 1\,]$). On the other hand, the variations of the controls decrease after using the redesigned helicopter, explaining the reduction in control energy when passive morphing is used.

B. Active Morphing

For the active morphing scenario only %5 change in trim values is permitted. For active morphing, in [12] helicopter models linearized around $V_A = 40$ kts straight level flight and some other flight conditions were used and the prescribed variance bounds on Euler angles were $\sigma^2 = 10^{-4}[\,1\ 1\ 0.1\,]$. The inputs of interest were all the conventional helicopter controls and the morphing controls. In this study we use $\sigma^2 = 10^{-6}[\,1\ 1\ 1\,]$ as prescribed variance constraints on Euler angles. After applying the active morphing design procedure, the relative energy saving is $\%J = \%84.1$ (also see Table II for optimal trim values). We remark that the value of the relative energy saving using active morphing was $\%J = \%84.6$ in [12]. Furthermore, using the actively morphing helicopter in [12] for the new OVC bounds (i.e. $\sigma^2 = 10^{-6}[\,1\ 1\ 1\,]$) the relative energy saving is $\%J = \%84.3$. These results illustrate two advantages of active morphing with respect to passive morphing. First, the relative energy savings are much higher when active morphing is used. Second, when active morphing is used the relative energy savings are very similar when different variance bounds for OVC are used. Therefore, the trade-off between relative control energy saving and satisfaction of more stringent comfort related variance constraints that we have seen when passive morphing was used is alleviated by active morphing.

TABLE II
Optimum Trim Variables

	Using Old Variance Bounds [12]		Using New Bounds	
	Optimum Value	Change $\Delta\Psi_{ai}/\Psi_{ai}$	Optimum Value	Change $\Delta\Psi_{ai}/\Psi_{ai}$
c_b	0.5664 m	0.04873	0.5644 m	0.04501
R	7.1250 m	−0.04999	7.1250 m	−0.04999
θ_{tw}	−0.1366 rad	−0.02455	−0.1467 rad	0.04785
Ω	25.6844 rad/s	−0.04873	25.7810 rad/s	−0.04515

For numerical simulations, the fourth closed-loop system is created using OVC designed with $\sigma^2 = 10^{-6}[\,1\ 1\ 1\,]$ for the actively morphing helicopter and coupling it to the corresponding actively morphing helicopter. Likewise, the fifth closed-loop system is created using OVC designed with $\sigma^2 = 10^{-4}[\,1\ 1\ 0.1\,]$ for the actively morphing helicopter and coupling it to the corresponding actively morphing helicopter. Lastly, the sixth closed-loop system is created using OVC designed with $\sigma^2 = 10^{-6}[\,1\ 1\ 1\,]$ for the nominal helicopter and coupling it to the nominal helicopter.

In Fig. 3, responses of ϕ_A, θ_0, and one of the morphing controls (i.e. R) are given when the fourth closed-loop system (solid black line) and fifth closed-loop system (dotted black line) are both excited by white noise perturbations. From this figure it can be easily seen that the variations of the Euler angles for the fourth closed-loop system are smaller than the ones for the fifth closed-loop system. This can be explained by the fact that the variance bounds of the fourth closed-loop system are smaller than the ones of the fifth closed-loop system. Note also that, similarly with the situation in Fig. 1, the variations of the Euler angles from their trim values are

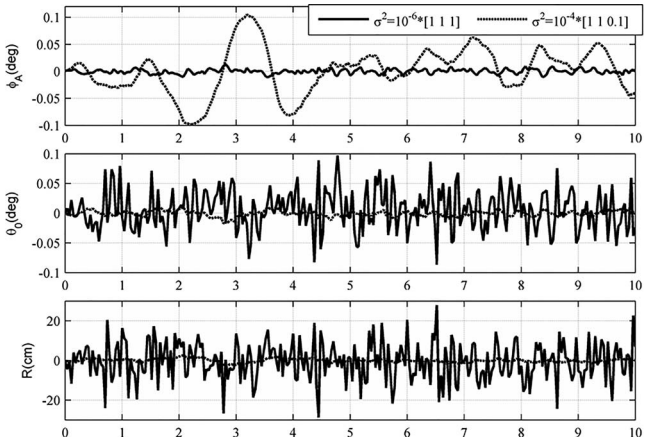

Fig. 3. Closed-loop responses of some perturbed states and controls using active morphing with different variance bounds (comfort version-I).

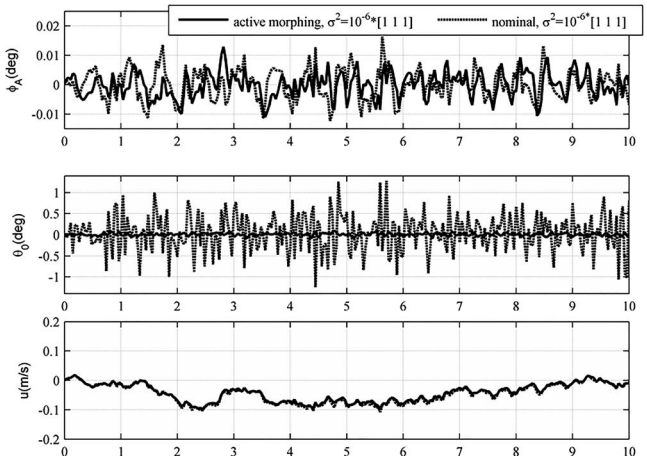

Fig. 4. Closed-loop responses of some perturbed states and controls using active morphing versus nominal helicopter (comfort version-I).

very small. It can also be seen that the control variations (e.g. θ_0) from their trim values increase after using new bounds (i.e. $\sigma^2 = 10^{-6}[\,1\ 1\ 1\,]$) since they are smaller than the old bounds (i.e. $\sigma^2 = 10^{-4}[\,1\ 1\ 0.1\,]$). This result confirms the fact that smaller variance bounds can be achieved with larger control inputs. The variations of morphing controls also increase when the variance bounds decrease. We remark by comparing Figs. 2 and 3 that the control effort required from the conventional controls decreases when active morphing is introduced because the morphing controls are now helping meet the objectives. We also note that the previous calculations refer to the relative control energy saving $\%J$, with respect to the nominal helicopter equipped with OVC designed to satisfy the respective output variance bounds (i.e. $\sigma^2 = 10^{-6}[\,1\ 1\ 1\,]$ and $\sigma^2 = 10^{-4}[\,1\ 1\ 0.1\,]$). Therefore, no confusion should arise from the fact that the relative control energy savings are similar whereas the control responses in Fig. 3 are different (the baseline for energy saving computation is different).

In Fig. 4, responses of ϕ_A, θ_0, and u are given when the fourth closed-loop system (solid black line) and sixth closed-loop system (dotted black line) are both excited by white noise perturbations. From this figure it can be seen that with and without active morphing, the qualitative (i.e., shape of the response) and quantitative (i.e. magnitude of the response) behaviors of helicopter Euler angles are practically the same. This is explained by the fact that the variances of outputs of interest (i.e., helicopter Euler angles) are very close and satisfy the same constraints. The variations of the controls decrease for the actively morphing helicopter. From Fig. 4 we also ascertain that other outputs (e.g. u) do not experience catastrophic behavior and their qualitative behavior is similar. This good behavior is explained by the exponentially stabilizing effect of OVC (see [9]).

V. VIBRATION/NOISE REDUCTION (COMFORT VERSION-II)

Amplitudes of flapping, lagging, and control angles are effective on comfortable helicopter flight, which becomes less noisy and less vibratory when these amplitudes are reduced. Therefore, in this section OVCs are designed for this purpose. The outputs of interest are three main flapping angles (i.e. collective and two cyclics) and three main lagging angles (i.e. collective and two cyclics). The inputs of interest are all helicopter controls. The number of inputs of interest is four for conventional helicopter and eight for the actively morphing helicopter. The output variance bounds on related angles are $\sigma^2 = a * 10^{-5}[\,1\ 1\ 1\ 1\ 1\ 1\,]$ where $a = 1$ for the conventional helicopter. Note that the selection of $a = 1$ was dictated by our numerical experiments. Specifically, it was impossible to satisfy output variance bounds with $a < 1$. However, it was possible to reduce that value of a in the case of the actively morphing helicopter, when a was chosen $a = 0.5$. This is expected because the actively morphing helicopter has more controls (eight) compared with the conventional one (four). The larger number of controls can be more effective both in satisfying output variance constraints and in reducing the control energy. Indeed, the energy saving after applying the active morphing idea is $\%J = \%97.6$ which is calculated using$100(0.9298 - 0.02125)/0.9298$.

For the vibration/noise reduction study two more closed-loop systems are created. The seventh closed-loop system is created using OVC designed with $\sigma^2 = 10^{-5}[\,1\ 1\ 1\ 1\ 1\ 1\,]$ for the nominal (i.e. nonmorphing) helicopter and coupling it to the nominal helicopter. The eighth closed-loop system is created using OVC designed with $\sigma^2 = 0.5 * 10^{-5}[\,1\ 1\ 1\ 1\ 1\ 1\,]$ for the actively morphing helicopter and coupling it to the actively morphing helicopter.

In Fig. 5 responses of some of the outputs of interest are given when the seventh closed-loop system (solid black line) and eighth closed-loop system (dotted black line) are both excited by white noise perturbations. From this figure the ability of OVC to practically suppress the new outputs can be ascertained: the variations of blade

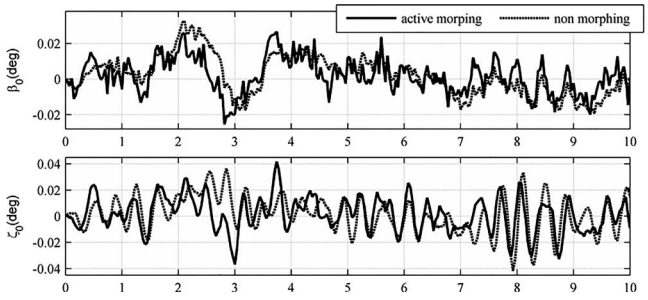

Fig. 5. Closed-loop responses of outputs of interest for nonmorphing vs actively morphing helicopter (comfort version-II).

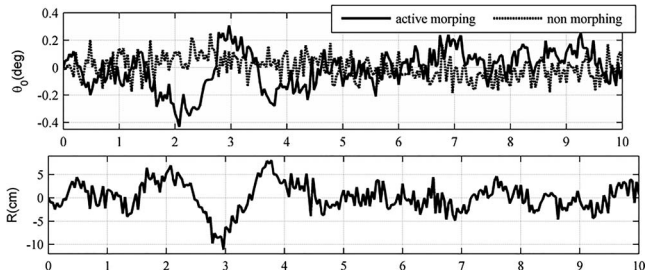

Fig. 6. Closed-loop responses of inputs of interest for nonmorphing vs actively morphing helicopters (comfort version-II).

flapping and lead-lagging angles from their trim values are very small because we used very small values for the output variance constraints in OVC design. Note also that because the difference between the output variance constraints is not as significant as in Figs. 1 and 2, the ranges of these variations are similar. In Fig. 6 responses of some inputs of interest are given when the seventh and eighth closed-loop systems are both excited by white noise perturbations. It can be seen that, in general, the variations of the conventional controls for the active morphing helicopter are smaller than the ones for the nonmorphing helicopter (only the blade pitch collective control behavior is in the same range as for the nonmorphing helicopter). However, our extensive analysis shows that the most important observation is related to the tail rotor control. For the nonmorphing helicopter, the tail rotor control exhibits much larger variations than all of the other controls. Therefore, for the nominal, nonmorphing helicopter, the tail rotor control is the dominant factor in the value of the control energy. However, when active morphing is used, the control effort required from the tail rotor decreases dramatically. Importantly, this is consistent with the physical intuition: in the nonmorphing helicopter the tail rotor control has to work, together with the other three conventional controls, towards a task it is not effective at: reducing the main rotor blade flapping and lead-lagging angles. However, when active morphing is used additional controls that act on the main rotor blade (and so are more effective at controlling blade flapping and lead lagging) are introduced. Therefore, these new controls relieve the tail rotor control from a task it is not adequate for. Moreover, additional controls due to active morphing do not experience large variations. This fact, in conjunction with the observation that the tail rotor control was the main contributor to the control energy in the nonmorphing helicopter, explains the large energy saving achieved via active morphing.

VI. CONCLUSIONS

Comfortable helicopter flight via passive/active morphing is investigated. Two comfortable flight types are considered. For the first comfort version, there are strict variance constraints on fuselage Euler angles that must be satisfied. For the second comfort version, strict variance constraints on blade flapping and lead-lagging angles must be satisfied.

For the first comfort version, when values very close to the achievable OVC variance bounds are used on Euler angles in passive morphing design, the control effort required is very large. Hence, while it is desired to use as small as possible bounds for improved comfort, a trade-off must be made between the control energy used for this purpose and the level of comfort achieved. When small but different output variance bounds are used in passive morphing design, a significant trade-off between the relative control energy saving obtained and level of comfort achieved is observed: satisfaction of stringent variance bounds leads to lower relative energy savings compared with the situation when less stringent bounds are satisfied. When active morphing is used for the same purpose (i.e., satisfaction of prescribed variance constraints on Euler angles) a much larger relative saving in control energy is observed. It is also observed that the trade-off between relative energy savings and the level of comfort is alleviated with respect to the passive morphing scenario.

For the second comfort version, when output variance constraints are prescribed on flapping and lead-lagging angles, active morphing results in a large relative energy saving with respect to the situation when morphing is not used (i.e. nonmorphing helicopter). Also, introduction of active morphing enables satisfaction of lower variance constraints on these angles. Importantly, introduction of active morphing controls results in a significant reduction of the tail rotor control effort, while not leading to large variations in the morphing controls, which explains the large energy saving observed when active morphing is used. Effectively the active morphing controls relieve the tail rotor from a task it is not effective at (i.e. main rotor blade flapping and lead-lagging control) at a relatively low control energy cost.

Numerical simulations of the closed-loop system responses for all scenarios considered indicated that the outputs of interest (i.e. Euler angles or blade flapping and lead-lagging angles) are practically suppressed when the closed-loop systems are excited by perturbations compatible with the ones used in the control design process. This is expected because very small values for output variance constraints are used in OVC design. It was

also observed that other outputs did not experience catastrophic behavior.

REFERENCES

[1] Edwards, B., and Cox, C.
Revolutionary concepts for helicopter noise reduction-SILENT Program. NASA-CR-2002-211650.

[2] Smith, E. C., Beale, M, Govindswamy, K., Vascsinec, M., and Lesieutre, G. A.
Aeroelastic response and stability of helicopters with elastomeric lag dampers.
Journal of American Helicopter Society, **41**, 3 (1996), 257–266.

[3] Glaz, B., Friedmann, P. P, and Liu, L.
Vibration reduction and performance enhancement of helicopter rotors using an active/passive approach.
In *49th AIAA/ASME/ASCE/ASC Structures, Structural Dynamics, and Materials Conference*, Schaumberg, IL, 2008.

[4] Liu, L., Friedmann, P. P, Kim, I., and Bernstein, D. S.
Simultaneous vibration reduction and performance enhancement in rotorcraft using actively controlled flaps.
In *American Helicopter Society 62nd Annual Forum*, Pheonix, AZ, 2006.

[5] Sim, W. B., Janakiram, R. D., and Lau, B. H.
Reduced in-plane, low frequency noise of an active flap rotor.
Journal of the American Helicopter Society, **59** (2014), 022002-1-022002-17.

[6] Ganguli, R.
Optimum design of a helicopter rotor for low vibration using aeroelastic analysis and response surface methods.
Journal of Sound and Vibration, **258**, 2 (2002), 327–344.

[7] Johnson, W.
Helicopter Theory. Princeton, NJ: Princeton University Press, 1994, ch. 17.

[8] Schmitz, F. H., Aggarwal, H. R., and Boxwell, D. A.
Prediction measurement of a low-frequency harmonic noise of hovering model helicopter rotor.
Journal of Aircraft, **37**, 5 (2000), 786–795.

[9] Oktay, T.
Constrained control of complex helicopter models.
Ph.D. dissertation, Virginia Tech, Blacksburg, VA, May 2012.

[10] Oktay, T., and Sultan, C.
Simultaneous helicopter and control-system design.
AIAA Journal of Aircraft, **50**, 3 (2013), 911–926.

[11] Oktay, T., and Sultan, C.
Integrated maneuvering helicopter model and controller design.
AIAA Guidance, Navigation and Control Conference, Minneapolis, MN, Aug. 2012.

[12] Oktay, T., and Sultan, C.
Flight control energy saving via helicopter rotor active morphing.
AIAA Journal of Aircraft, **51**, 6 (2014), 17841804.

[13] Fusato, D., Guglieri, G., and Celi, R.
Flight dynamics of an articulated rotor helicopter with an external slung-load.
Journal of the American Helicopter Society, **46**, 1 (2001), 3–14.

[14] Fusato, F., and Celi, R.
Multidisciplinary design optimization for helicopter aeromechanics and handling qualities.
Journal of Aircraft, **43**, 1 (2006), 241–252.

[15] Gong, H., Zhen, Z., Lin, X., Jiang, J., and Wang, X.
Design of automatic climbing controller for large civil aircraft.
Journal of the Franklin Institute, **350** (2013), 2442–2454.

[16] Barczyk, M.
Integration of a triaxial magnetometer into a helicopter UAV GPS-aided INS.
IEEE Transactions on Aerospace and Electronic Systems, **48**, 4 (2012), 2947–2960.

[17] Andrisani, D., Kim, E. T., Schierman, J., and Kuhl, F. P.
A nonlinear helicopter tracker using attitude measurements.
IEEE Transactions on Aerospace and Electronic Systems, **27**, 1 (1991), 40–47.

[18] Carrillo, L. R. G., Dzull, A., and Lozano, R.
Hovering quad-rotor control: A comparison of nonlinear controllers using visual feedback.
IEEE Transactions on Aerospace and Electronic Systems, **48**, 4 (2012), 3159–3170.

[19] Zarei, J., Montazeri, A., Motlagh, M. R. J., and Poshtan, J.
Design and comparison of LQG/LTR and H_∞ controllers for a VSTOL flight control system.
Journal of the Franklin Institute, **344** (2007), 577–594.

[20] Bo, L. Y., Zhu, L. W., and Qi, S.
Improved LQG control for small unmanned helicopter based on active model in uncertain environment.
In *International Conference on Electronics, Communications and Control (ICECC)*, Ningbo, China, 2011.

[21] Park, S., Bae, J., Kim, Y., and Kim, S.
Fault tolerant flight control system for the tilt-rotor UAV.
Journal of the Franklin Institute, **350** (2013), 2535–2559.

[22] Luo, C. C., Liu, R. F., Yang, C. D., and Chang, Y. H.
control design with robust flying quality.
Aerospace Science and Technology, **7** (2003), 159–169.

[23] Kureemun, R., Walker, D. J., Manimala, B., and Voskuijl, M.
Helicopter flight control law design using techniques.
In *Proceedings of the 44th IEEE Conference on Decision and Control and the European Control Conference 2005*, Seville, Spain.

[24] Kung, C. C.
Nonlinear robust control applied to F-16 aircraft with mass uncertainty using control surface inverse algorithm.
Journal of the Franklin Institute, **345** (2008), 851–876.

[25] Bogdanov, A. A., and Wan, E. A.
Model predictive neural control of a high-fidelity helicopter model.
In *AIAA Guidance Navigation and Control Conference*, Montreal, Canada, 2001.

[26] Gibbens, P. W., and Megagoda, E. D. B.
Efficient model predictive control algorithm for aircraft.
Journal of Guidance, Control, and Dynamics, **34**, 6 (2011), 1909–1915.

[27] Dalamagkidis, K., Valavanis, K. P., and Piegl, L. A.
Nonlinear model predictive control with neural network optimization for autonomous autorotation of small unmanned helicopters.
IEEE Transactions on Control Systems Technology, **19**, 4 (2010), 1–14.

[28] Oktay, T., and Sultan, C.
Variance constrained control of maneuvering helicopters with sensor failure.
In *Proceedings of the IMechE, Part G: Journal of Aerospace Engineering*, **227**, 12 (2013), 1845–1858.

[29] Oktay, T., and Sultan, C.
Modeling and control of a helicopter slung-load system.
Aerospace Science and Technology, **29**, 1 (2013), 206–222.

[30] Oktay, T., and Sultan, C.
Variance constrained control of maneuvering helicopters.
In *American Helicopter Society 68th Annual Forum*, May 2012.

[31] Oktay, T., and Sultan, C.
Robustness of variance constrained controllers for complex helicopter models.
In *American Control Conference*, June 2013.

[32] Oktay, T.
Performance of minimum energy controllers on tiltrotor aircraft.
Aircraft Engineering and Aerospace Technology, **86**, 5 (2014).

[33] Castillo, P., Munoz, L. E., and Santos, O.
Robust control algorithm for a rotorcraft disturbed by crosswind.
IEEE Transactions on Aerospace and Electronic Systems, **50**, 1 (2014), 756–763.

[34] Skelton, R. E.
Dynamic Systems Control: Linear Systems Analysis and Synthesis. New York: Wiley, 1987, ch. 8.

[35] Skelton, R. E., Iwasaki, T., and Grigoriadis, K.
A Unified Algebraic Approach to Linear Control Design. New York: Taylor & Francis, 1998, ch. 4.

[36] Skelton, R. E., and Lorenzo, M. D.
Space structure control design by variance assignment.
Journal of Guidance, Control, and Dynamics, **8**, 4 (1985), 454–462.

[37] Skelton, R. E., and Sultan, C.
Controllable tensegrity, A new class of smart structures.
In *SPIE International Symposium on Smart Structures and Materials*, San Diego, CA, 1997.

[38] Sultan, C., and Skelton, R. E.
Integrated design of controllable tensegrity structures.
In *ASME International Mechanical Engineering Congress and Exposition*, Dallas, TX, 1997.

[39] Wagtendonk, W. J.
Principles of Helicopter Flight (2nd ed.). Aviation Supplies & Academics, Inc., Newcastle, WA, 2006, p. 77.

[40] Spall, J. C.
Multivariable stochastic approximation using a simultaneous perturbation gradient approximation.
IEEE Transactions on Automatic Control, **37** (1992), 332–341.

[41] Sultan, C.
Proportional damping approximation using the energy gain and simultaneous perturbation stochastic approximation.
Mechanical Systems and Signal Processing, **24** (2010), 2210–2224.

[42] Padfield, G. D.
Helicopter Flight Dynamics (2nd ed.) (AIAA Education Series). New York: Wiley, 2007, pp. 265–267.

[43] Leishman, J. G.
Principles of Helicopter Aerodynamics. New York: Cambridge University Press, 2006, p. 160.

[44] Oktay, T., and Sultan, C.
Constrained predictive control of helicopters.
Journal of Aircraft Engineering and Aerospace Technology, **85**, 1 (2013).

[45] Hsieh, C., Skelton, R. E., and Damra, F. M.
Minimum energy controllers with inequality constraints on output variances.
Optimal Control Application and Methods, **10**, 4 (1989), 347–366.

[46] Zhu, G., and Skelton,
R. E. Mixed L_2 and L_∞ problems by weight selection in quadratic optimal control.
International Journal of Quadratic Optimal Control, **63**, 5 (1991), 1161–1176.

[47] Sultan, C.
Decoupling approximation design using the peak to peak gain.
Mechanical Systems and Signal Processing, **36**, 2 (2013), 582–603.

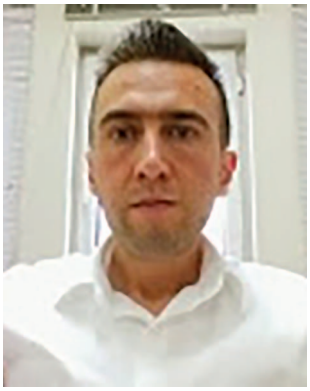

Tugrul Oktay received an M.S. degree in aeronautical and astronautical engineering from Istanbul Technical University, 2008, and a Ph.D. degree in aerospace engineering in the Aerospace and Ocean Engineering Department at Virginia Tech, 2012. He had a scholarship from the Ministry of National Education, Republic of Turkey.

Dr. Oktay has more than 20 technical papers in his areas of research interests.

Cornel Sultan holds an M.S. degree in mathematics, and a Ph.D. degree in aerospace engineering from Purdue University, West Lafayette, IN (1999).

He has been affiliated with a start-up company, Tensegra Inc. (1999-2001), Harvard Medical School (2001-2003), Scientific Systems (2001-2004), and United Technologies Research Center (2004-2007). Currently he is an associate professor in the Aerospace and Ocean Engineering Department at Virginia Tech. His current research interests are in tensegrity and membrane structures, rotorcraft, and coordinated vehicles.